AAPS PharmSciTech, Vol. 14, No. 1, March 2013 (© 2012)
DOI: 10.1208/s12249-012-9910-4

Research Article

Monitoring Blending of Pharmaceutical Powders with Multipoint NIR Spectroscopy

Otto Scheibelhofer,[1] Nikolaus Balak,[1] Patrick R. Wahl,[1] Daniel M. Koller,[1] Benjamin J. Glasser,[2] and Johannes. G. Khinast[1,3,4]

Received 16 August 2012; accepted 7 December 2012; published online 21 December 2012

Abstract. Blending of powders is a crucial step in the production of pharmaceutical solid dosage forms. The active pharmaceutical ingredient (API) is often a powder that is blended with other powders (excipients) in order to produce tablets. The blending efficiency is influenced by several external factors, such as the desired degree of homogeneity and the required blending time, which mainly depend on the properties of the blended materials and on the geometry of the blender. This experimental study investigates the mixing behavior of acetyl salicylic acid as an API and α-lactose monohydrate as an excipient for different filling orders and filling levels in a blender. A multiple near-infrared probe setup on a laboratory-scale blender is used to observe the powder composition quasi-simultaneously and in-line in up to six different positions of the blender. Partial least squares regression modeling was used for a quantitative analysis of the powder compositions in the different measurement positions. The end point for the investigated mixtures and measurement positions was determined *via* moving block standard deviation. Observing blending in different positions helped to detect good and poor mixing positions inside the blender that are affected by convective and diffusive mixing.

KEY WORDS: blender geometry; multiprobe measurement; multivariate analysis; near-infrared spectroscopy; powder mixing dynamics; quantitative continuous monitoring.

INTRODUCTION

Blending is a critical unit operation in pharmaceutical manufacturing, as it is a prerequisite for the homogenous distribution of a drug's components. Clearly, the content of the active pharmaceutical ingredients (API) in the final solid dosage form is particularly important. Tablets out of specifications lead to expensive rework or even recalls, and even more important, dosage forms not compliant with the therapeutic window may cause harm to patients. Another crucial feature affected by powder homogeneity is downstream processability (*i.e.*, compaction of tablets may lead to problems, if certain components are distributed unevenly, *e.g.*, during lubrication with magnesium stearate (1,2)).

Two main mechanisms are responsible for blending. The first mechanism is due to convective transport, which is the transport of large volumes imposed by the blender (3). It is fast, is influenced mainly by the geometry of the blender, and generates homogeneity on a large scale. The direction of mixing is aligned with the direction of the particle moving. Indirectly, shear mixing is an outcome of convective transport. The second mechanism is diffusive blending, which is a result of the individual particle movement with respect to the convectively transported particle collective. Here, mixing also occurs perpendicular to the direction of the flow. It is slower and based on the particle mobility, *i.e.*, diffusivity. Diffusive blending, which is strongly influenced by cohesion of the components, delivers homogeneity on a small scale (4,5).

Competing with the powder mixing process is segregation—or demixing—which always exists, if the individual particles do not have identical properties. Segregation occurs for several reasons, such as differences in density, size, shape, surface properties, friction coefficients, and other physical parameters. Often, the API is crystallized and dried to form small drug crystals (6,7) that are blended with larger excipient particles. Even small size differences can lead to segregation, and in general, segregation effects are difficult to quantify and to predict as they are a complex function of the previously mentioned parameters. For example, small and large cohesive forces increase segregation, while intermediate cohesivity is beneficial for suppressing segregation. In summary, the final state of a blend is in equilibrium between mixing and segregation. Segregation can, therefore, alter blending times or even prohibit a homogenous blend (5,8,9).

In industrial practice, the quality of blending is often determined by invasive thief sampling, followed by an off-line chemical analysis of the sampled material. Another method is near-infrared (NIR) spectroscopy that allows noninvasive and in-line measurements. In addition, diverse chemical and,

[1] Research Center Pharmaceutical Engineering GmbH, Graz, Austria.
[2] Department of Chemical and Biochemical Engineering, Rutgers University, Piscataway, New Jersey, USA.
[3] Institute for Particle and Process Engineering, Graz University of Technology, Inffeldgasse 21a, 8010, Graz, Austria.
[4] To whom correspondence should be addressed. (e-mail: khinast@tugraz.at)

under certain circumstances, physical parameters can be monitored *via* NIR. By combining NIR spectroscopy and multivariate methods, critical quality characteristics of powders and solid dosage forms can be extracted in a straightforward manner (10). Many pharmaceutical processes are relatively easily accessible using NIR in combination with fiber optics (11–13). They can be monitored without changing the process setup and barely require manual effort (14,15). For example, the monitoring of a components' concentration on a quantitative basis during blending has been successfully performed (16–19). Overcoming the problems associated with differences between calibration and measurement has been discussed in the literature (20,21). Moreover, the dynamics of blending processes have been studied theoretically as well (22,23) and experimentally using model substances (24) and pharmaceutical powders (25). However, using one probe in the same position usually does not provide a reliable assessment of the blending process (21,26).

In our study, we used a multiprobe NIR setup to monitor the blending process in up to six different positions, providing a much clearer picture of what occurred during the processes and how the components were distributed inside the blending vessel.

Replication experiments showed that the same dynamics were present inside the vessel under the same conditions. Thus, experiments were reproducible. In addition, the loading protocol of the vessel was varied in order to monitor the emergence of two blending regimes. Fast blending, which was observed for low fill levels and near the impeller, was affected by segregation. Slow blending, which was detected for high fill levels and far from the impeller, took longer to approximate the homogenous mixture.

In summary, our study shows that monitoring only one position in the powder blender may lead to misinterpretations of the blending status.

MATERIALS AND METHODS

Materials

For the experiments, two powders with different properties were used. Acetyl salicylic acid (ASA) Rhodine© from Rhodia Group (La Défense, France) was used as model API. ASA forms rod-shaped crystals, as shown in Fig. 1. α-Lactose monohydrate (LM) Tablettose 80© from Meggle GmbH (Wasserburg, Germany) was used as an excipient. Tablettose is granulated LM, which forms close to spherical particles.

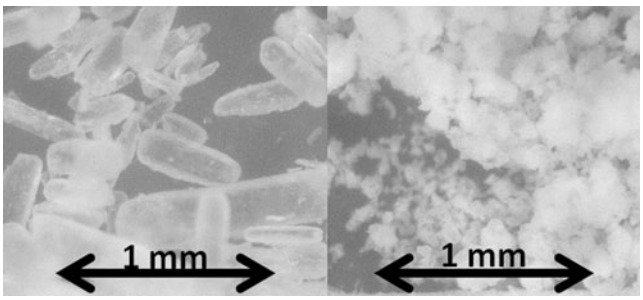

Fig. 1. Microscopic images captured with a reflected light microscope (Wild Heerbrugg). *Left* ASA, *right* LM

Q_3 size distribution (*i.e.*, the volume density distribution) of the particles was monitored *via* a QICPIC system combined with a dry disperser RODOS/L and a vibratory feeder VIBRI/L (all by Sympatec GmbH, Clausthal-Zellerfeld, Germany). In this method, the dispersed particles are imaged by a high-speed camera. The size of the particles is estimated based on the images by using the equivalent projected circle diameter (27). A summary of the Q_3 distribution measures is shown in Table I. The errors were estimated by three consecutive measurements of about 2 g of each powder.

Experimental Setup

A stainless steel vessel with a speed-controlled four-bladed impeller was used for the blending experiments. The gear motor was a Heidolph RZR 2102 from Heidolph Instruments (Schwabach, Germany). This setup is a simplified model system for agitated industrial blenders and may be seen as a scaled-down version of high-shear mixers or filter-bed dryers.

The vessel had ten NIR measurement ports (three at the bottom and seven at the wall) that could be used for process monitoring, as schematically illustrated in Fig. 2. The optical probes used for illumination and detection had bifurcated fibers with a core diameter of 600 μm each. The fibers were connected to a fiber switch (FSM2 (1×6), piezosystem jena GmbH, Jena, Germany), which allows measurement of the powder composition in up to six different positions. From each probe position, the signal was transferred to an FT-NIR-spectrometer (Spectrum™ 400, PerkinElmer, Waltham, Massachusetts, USA). The fill levels of the vessel are denoted as the ratio of the (approximate) powder height to the vessel diameter. The investigated fill levels are shown in Fig. 2 as dashed lines.

All experiments had an identical setup. The first component was loaded into the empty vessel. Next, the impeller was inserted and positioned 1 mm above the bottom of the vessel. Finally, the second component was loaded into the vessel.

Several experiments with the same composition and fill order were performed to investigate reproducibility. Seventy grams of LM were loaded on top of 70 g of ASA (resulting in a height to diameter ratio $[H/D]$=0.35). Positions 1, 2, and 3 were at the bottom of the vessel. They were separated from the blade by a layer of powder. As can be seen, position 3 was a critical location, as it was located directly at the edge of the vessel. Position 4 was on the side wall, at the height of the impeller blades, which affected the measurement signals. The integration time of the spectra was optimized to reduce this effect, but it still resulted in a larger confidence interval at this position. Position 5 was above the blade and position 6 was slightly under the powder fill level.

Table I. Q_3 Particle Size Distribution of the Used Powders

	d_{10} (μm)	d_{50} (μm)	d_{90} (μm)
Acetyl salicylic acid	252±4	439±9	725±25
α-Lactose monohydrate	76±1	191±3	420±6

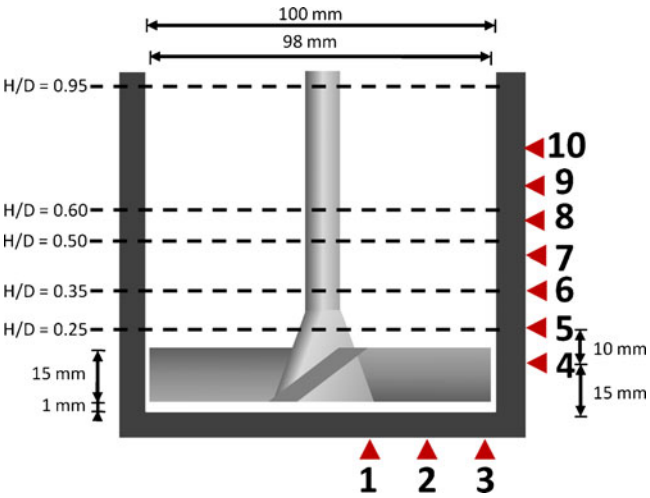

Fig. 2. Schematic illustration of the blending vessel. Measurement ports *1–10* for the optical fibers are indicated by the *arrows*. The *dashed lines* indicate the investigated fill levels

Calibration

To estimate the API concentration, a partial least squares (PLS) model was developed. The previously mentioned powders tend to segregate, as described in the literature (25). Typically, ASA particles rise to the top due to their larger size. Thus, calibration inside the blending vessel is not possible. An alternative novel calibration setup using a moving disk (see succeeding paragraphs) was, therefore, developed.

However, due to the difference between calibration and in-line measurements inside the vessel, spectral pretreatments had to be applied to filter out factors associated with the differences in the measurement geometries. In this work, we used TheUnscrambler® 9.8 (Camo, Oslo, Norway) to perform the spectral pretreatments and PLS.

Difference Between Calibration and Measurement

For calibration, premixed blends were prepared in a tumbling blender (Turbula T2F, Willy A. Bachofen AG Maschinenfabrik, Muttenz, Switzerland) for 20 min at 50 rpm to ensure homogeneity. Blends with API contents of 0%, 5%, 10%, 20%, 30%, 40%, 45%, 50%, 55%, 60%, 70%, 80%, 90%, 95%, and 100% (*w*/*w*) were made for calibration. The premixes were placed on a rotating disk as a thick layer of powder. The optical fibers were positioned above the disk, about 1 mm above the moving powder bed and 2.55 cm off the center. Spectra were recorded when the disk with the premixes rotated (at 15 rpm) with respect to the fiber optic probes.

The following differences between the calibration and in-line measurements were observed:

- Although the powders were moving in both cases (*i.e.*, rotating disk and blender vessel), ensuring that the sampled powder mass was sufficiently high, the speed at which the powders were passing through the incident beam of the optical fibers was different.
- During blender measurements, there was a sapphire window separating the fiber from the vessel interior, whereas during calibration, there was a small gap of air to prevent powder segregation due to the probes.
- The optical fibers were bent slightly differently, which might have led to artificial absorption bands in the spectra.

Spectral Acquisition and Pretreatment

Spectral pretreatment was applied to separate the chemical signature contained in the signal from the physical interferences due to differences in the geometries and measurement conditions. The spectra were recorded with the Spectrum™ 400 FT-NIR-spectrometer within the range of 10,000–4,100 cm^{-1} and a resolution of 16 cm^{-1}. For every measurement point, 12 recorded spectra were integrated, and then the switch proceeded to the next fiber. As a result, the integration time for one spectrum in one position was roughly 4.2 s. The same position was measured again after 25.2 s (=4.2 s×6).

The following spectral preprocessing methods were used in combination since they enhance the spectral information related to capturing the blend evolution and powder properties. They also gave the best predictive power for the developed models.

- When exporting the spectra, intermediate points are interpolated automatically by the software of the spectrometer, giving a resolution of 2 cm^{-1}. To avoid dealing with that unnecessarily large amount of correlated data, eight measurement points were averaged again, restoring the range of 16 cm^{-1}. Thus, the final number of spectral points is 368.
- Performing a standard normal variate (SNV) of the spectra within the range of 10,000–4,560 cm^{-1}. The cutoff at the low-energy end of the recorded spectra was chosen to ignore the region where the optical fibers cut the signal. SNV was performed as follows:

$$a_{i,\mathrm{SNV}} = \frac{a_i - \overline{a}}{\sqrt{\frac{1}{k-1}\sum_{j=1}^{k}\left(a_j - \overline{a}\right)^2}}$$

  where a_i is the absorbance at the wavelength λ_i and $\overline{a}$ is the arithmetic mean of all a_i (28).
- The region above 7,226 cm^{-1} does not contain any of the constituents' chemical signatures and was, therefore, neglected. This leaves the region of 7,226–4,560 cm^{-1}, containing the (partly overlapping) specific bands of ASA and LM, which were used for further analysis.

A principal component analysis (PCA) was carried out to determine the differences between the calibration and in-line spectra. Under PCA, the investigated data variables (the spectra in our case) are projected onto a space, whose axes are the principal components (PCs); PCs are linear combinations of the measured variables, and each PC captures the directions of maximum variance in the measured data (28). These projected values, termed scores, are shown in Fig. 3.

Every spectral measurement of the calibration samples is represented in Fig. 3 by a colored dot. Overall, the calibration

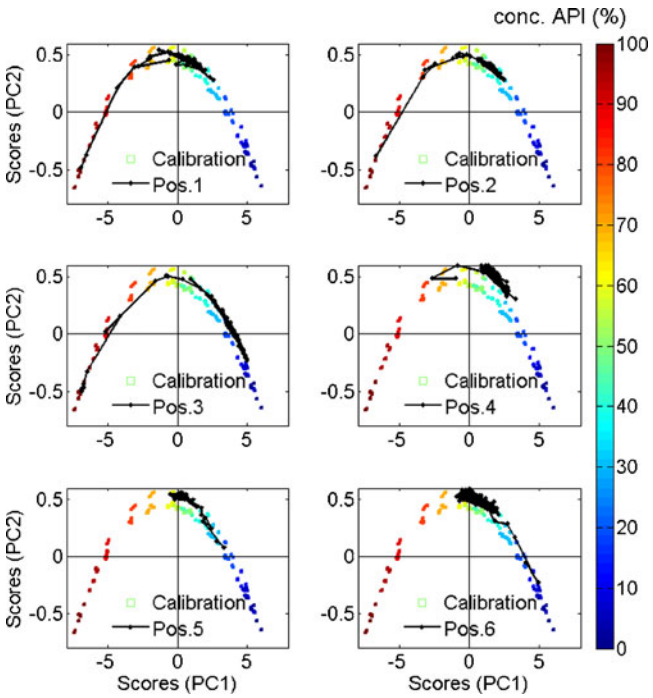

Fig. 3. Score trajectory curve. *Colored dots* represent the calibration spectra. Color is chosen corresponding to the fraction of API (see the *color bar*). *Black dots* represent the in-line spectra. Consecutively measured in-line spectra at one position are connected by *black lines* to show the change in the scores with blending time. The first PC (*horizontal axis*) explains 98% of the calibration and 89% of the in-line data. The second PC (*vertical axis*) explains 1% of the calibration and 3% of the in-line data

samples are arranged in the form of an arch, ranging from 0% at the right end to 100% at the left end of the arch.

Superimposed on this is a typical blending experiment with 50% (*w*/*w*) of LM on top of 50% (*w*/*w*) ASA. This corresponds to a fill level of H/D=0.35. The rationale behind choosing equal fractions of each component is to have the highest sensitivity towards detecting small changes in the powder bed for both constituents.

These in-line measurements are represented by the line-connected points. Different measurement positions originated in the different positions in the score plot due to their different initial concentrations of ASA. However, they stay on the same curve as the calibration samples and end up at 50% concentration of ASA, indicating that steady state was reached where all positions showed similar spectra. Moreover, the in-line measurements follow the same trajectory in scores on the arch as the calibration measurements. This means that the model was not affected by the difference in spectral acquisition. However, the points representing the spectra measured in position 4 were slightly off the trajectory. Changing the position of the impeller made it clear that the deviation originated from the impeller blade, which in this case was in front of position 4.

Calibration Based on Single vs. Multiple Probes

The PLS that was used to set up the calibration is a widely used algorithm to estimate a response variable y based on the known measured variables X by calibrating with known samples. The measurements are projected on latent variables, which represent the structure of the measurements. They are then connected to the response variable *via* an assumed and iteratively improved linear relationship. The resulting regression coefficients can be used to estimate the response variable for unknown samples (29). In our case, X was represented by the measured and pretreated spectra and y was the API concentration.

The multiprobe measurement system allows two different approaches for developing a predictive model: (1) a model for every single probe (*i.e.*, for each of the six measurement probes) and (2) a general model for all six probes, which incorporates all calibration data of the different probes. A distinct model for every channel takes fiber-specific influences into consideration, which can be everything in the light path, ranging from the fiber switch to the probe, including the unique bending of the fibers. In contrast, a general model incorporates all of these effects in one global model. Although the predictions may be less specific with respect to individual channels, this model is more robust since all the disturbances are accounted for and unknown but similar disturbances have little effect on the predictions.

The quality of the model is often estimated by the residual mean square error of calibration (RMSEC), which is derived *via* the following formula (28), where $\hat{y}_i$ is the predicted concentration, y_i is the reference concentration, and n is the number of samples:

$$\mathrm{RMSEC} = \sqrt{\frac{\sum_{i=1}^{n}(\hat{y}_i - y_i)^2}{n}}$$

This is graphically shown in Fig. 4. The reference and predicted values are plotted against each other in the so-called observed *vs.* predicted plot for the general model.

To examine the robustness of the models, cross-validation was used. Groups of the samples with the same component concentration were formed. One group was left out, and a model was created without this group. Then, the concentration in this group was predicted by the model. This was

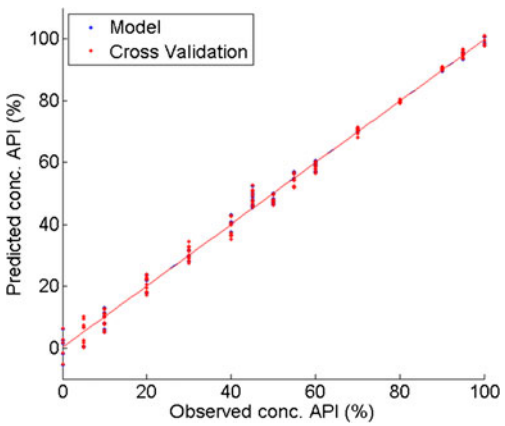

Fig. 4. Observed *vs.* predicted plot of the overall PLS regression model predicting the API concentration. The *red points* represent the actual model; the *blue points* are obtained *via* cross-validation. The best-fit line was plotted for both. The statistics are shown in Table II

performed for every group to determine the residual mean square error of cross-validation (RMSECV).

The statistics of single-probe and general models are summarized in Table II. The models were based on the same original data and consist of two PLS components. The statistical summary for the regression models and the cross-validated models indicate that the single-probe models seem to perform better. However, the confidence intervals on the predicted values in the in-line experiments, as shown in Fig. 5, indicate a different behavior. For the calculation of the confidence intervals, it is taken into account how good the PLS models, based on off-line spectra, can reflect the newly gained in-line spectra. Unexplained differences between in-line and off-line spectra lead to a larger confidence interval. Hence, the confidence intervals give a more reliable estimation of the models' reliability.

A typical blending experiment predicted by the single-probe models and the general model is shown in Fig. 5. As can be seen, the confidence interval is larger in the single-probe models compared to the general model (with the notable exception in position 4, where the passing impeller influenced the measurement). A greater confidence interval typically suggests that there are unexplained differences between calibration and in-line measurements, leading to uncertainties in predictions. In our case, this may be due to the different bending of the fibers for calibration and in-line measurements. We, therefore, opted for the general probe model.

Determining Blending Dynamics, End Point, and Homogeneity

In principle, two main questions arise during blending processes: (1) has the blending process reached its end point (*i.e.*, can the blend quality be improved by further blending) and (2) is the blend homogenous?

To determine if the blending process reached the end point, variations between consecutive spectra are often used, applying moving block standard deviation (MBSD). This is done by (1) calculation of the standard deviations for all wavelengths in the region of interest across a block of several consecutive spectra; (2) calculation of the arithmetic mean of these standard deviations, this is the MBSD value at a certain time step; (3) now the oldest spectrum is removed and the next current one added, this is repeated until the process ends. If the MBSD value drops below a certain threshold, the blend may be regarded as stationary and its composition will remain unchanged on the time scale of interest (16,30).

The size of the volume V, which is represented by one measurement point, was estimated as $V = \omega \times 2\pi \times r \times t \times n \times d \times f \times k \approx 30\ \text{mm}^3$ with the speed of the impeller ω= 4.5 rpm, the radius of the vessel r=5 cm, the time for one spectra collected t=0.35 s, the number of spectra accumulated n=12, the NIR penetration depth in the pharmaceutical compounds d=0.5 mm, the diameter of the optical fiber f=600 μm, and the factor for the ratio of speed between the powder and blade assumed to be k=1. Note that only a fraction of the whole powder volume was analyzed, and thus, the sum of all measurement positions did not have to be 100%.

Another important issue of powder blending processes is the blending dynamics, which can be evaluated *via* a method that is similar to MBSD. In our approach, the MBSD methodology is applied to the PLS predictions instead of the raw spectra. Therefore, the weighting of certain spectral regions, as defined in the PLS coefficient vector, was conserved. This

Table II. Summary of the Model Statistics for the Single-Probe Calibration and General Models

	Slope	Offset (%)	RMSE (%)	R^2
Position 1	0.999	0.051	0.876	0.999
	1.001	−0.105	1.079	0.999
Position 2	0.998	0.088	1.334	0.998
	0.998	0.108	1.477	0.998
Position 3	0.996	0.196	1.985	0.996
	0.994	0.250	2.161	0.996
Position 4	0.998	0.105	1.456	0.998
	0.996	0.187	1.592	0.998
Position 5	0.998	0.103	1.438	0.998
	0.999	0.042	1.555	0.998
Position 6	0.998	0.120	1.553	0.998
	0.997	0.148	1.700	0.997
Overall	0.995	0.269	2.298	0.995
	0.994	0.270	2.407	0.995

The first line provides the model statistics and RMSEC, and the second line shows the statistics obtained *via* cross-validation and RMSECV

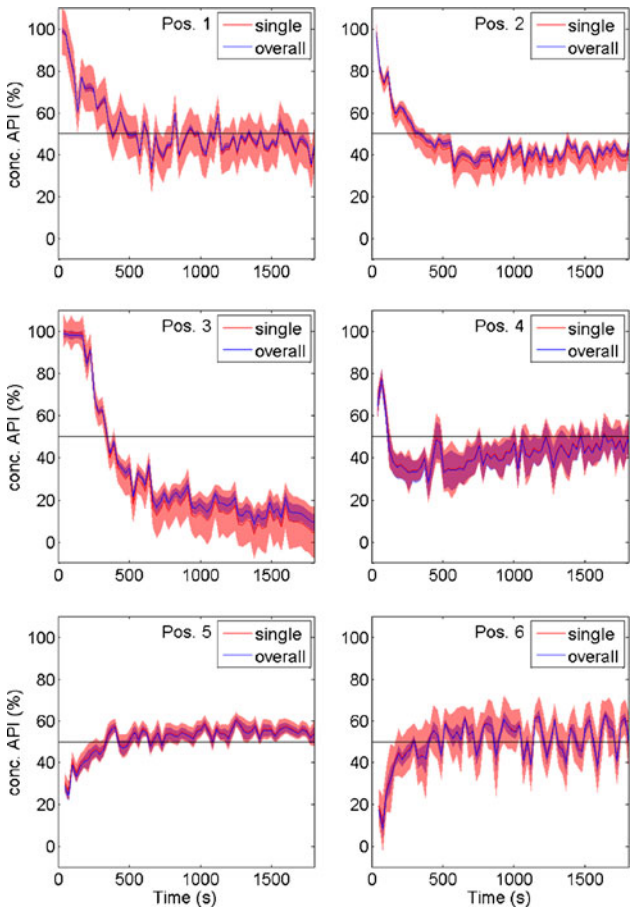

Fig. 5. The same experiment predicted with the single-probe and general models. The single-probe models are shown in *red* and the 95% confidence interval for the predictions is illustrated by the *red-shaded area*. The predictions of the overall model are represented by the *blue line* and 95% confidence interval by the *blue-shaded area*. This is the same experiment as in Fig. 3

strategy was chosen since the deviations that may have been induced by the movement of the powder (which can be seen in the raw spectra), but do not give any information about the composition, were reduced in the PLS. Before employing MBSD, a Savitzky–Golay smoothing was applied to the predictions, with a window of nine points and a second-order polynomial to minimize short-term fluctuations. A window size of eight measurement points was chosen to calculate the MBSD as this reflects three times the volume of the standard dosage form (for a tablet of 6 mm in diameter and 3 mm in height).

RESULTS AND DISCUSSION

Reproducibility of Experiments

Three runs with the same composition and fill order were performed to study the reproducibility of our setup. The predictions made using the PLS model are shown in Fig. 6. Positions 1, 2, and 3 were at the bottom of the vessel.

As pointed out previously, at the beginning of the experiment, pure ASA was at the bottom and in the lower part of the vessel (positions 1–4), whereas LM was in the upper part of the vessel (positions 5 and 6). As can be seen in Fig. 6, the API concentration decreased to approximately 50% (the final value for a perfect mixture) at positions 1 and 2 at the bottom of the vessel and seemed to reach a homogeneous state within roughly 500 s.

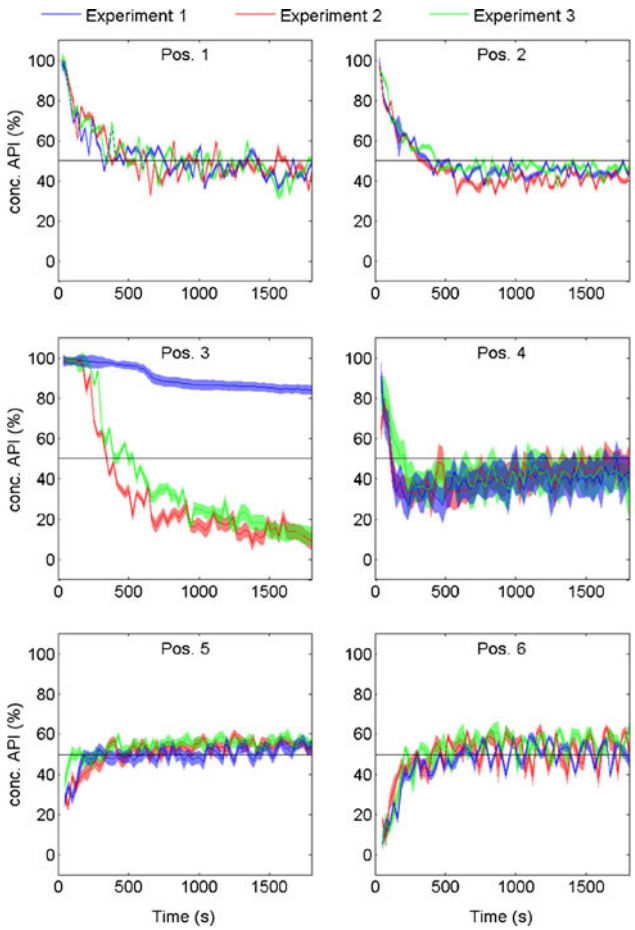

Fig. 6. Seventy grams of LM was deposited on 70 g of ASA (resulting in H/D=0.35). The experiment was repeated three times. The *solid lines* show the predicted API values, and the *transparent area* represents the respective 95% confidence interval of the prediction. The *black line* indicates the nominal value. Positions higher than 6 were above the powder fill level

At position 3 in the corner of the blending vessel, the API concentration decreased as well. However, in two out of three experiments, it reached a much lower value, while in the third experiment, just a slight decrease occurred. In addition, different experiments showed a different trajectory. Thus, some segregation occurred and powder seems to have stuck to the wall at these positions. Additionally, there were random events, *e.g.*, when powder gets stuck and is removed again. Hence, these positions are critical for mixing and powder stuck to the wall should not be emptied into the processing container after blending, unless it is deemed negligible in amount. Note, however, that if a large amount of a specific material selectively sticks to the wall (*e.g.*, in small blenders with a high surface-to-volume ratio), the overall blend composition may be significantly affected.

Position 4 showed an interesting behavior, as it started with pure ASA. However, LM quickly concentrated at this position (overshoot) and it reached a final steady state of about 50% only after many revolutions. This seems to indicate that ASA at the bottom of the vessel was pushed upwards by the blade, to the region above the blade, and trickled down afterwards. Positions 5 and 6 showed a decrease in LM and an increase in ASA concentrations. Position 6, which was the highest, showed a slower convergence to the nominal state. However, the convergence to the steady state was faster at these positions compared to positions 1 and 2.

Overall, the experiments show fluctuations in the order of 10% API in the range of 100 s. This was a real effect due to a small sample size but could be observed for the whole duration of the experiments.

Influence of Loading Order

Since the two materials showed significant differences in particle size and shape, variations in the mixing time and performance were expected, depending on the loading order. Therefore, experiments with reversed loading order, *i.e.*, 70 g of ASA on top of 70 g of LM, were performed. They were repeated three times to test the reproducibility of the results. The results are presented in Fig. 7.

As before, similar mixing dynamics were observed. However, there were some differences. For position 4, which was covered with LM in the beginning, the previously observed overshoot did not appear. The ASA was only transported down (and LM up). Moreover, the blending time until homogeneity in the lower part of the vessel was reached was significantly increased. In contrast, the mixing in the top part of the vessel was faster. For channel 3, the deposition of powder was observed again.

As in the previous experiments, we observed that there was more than the expected concentration (*i.e.*, 50%) of ASA in the upper half of the vessel and less in the lower part, indicating the segregation tendencies of the two-component system ASA and LM. However, in the latter experiments (ASA on top), the effect was slightly more pronounced.

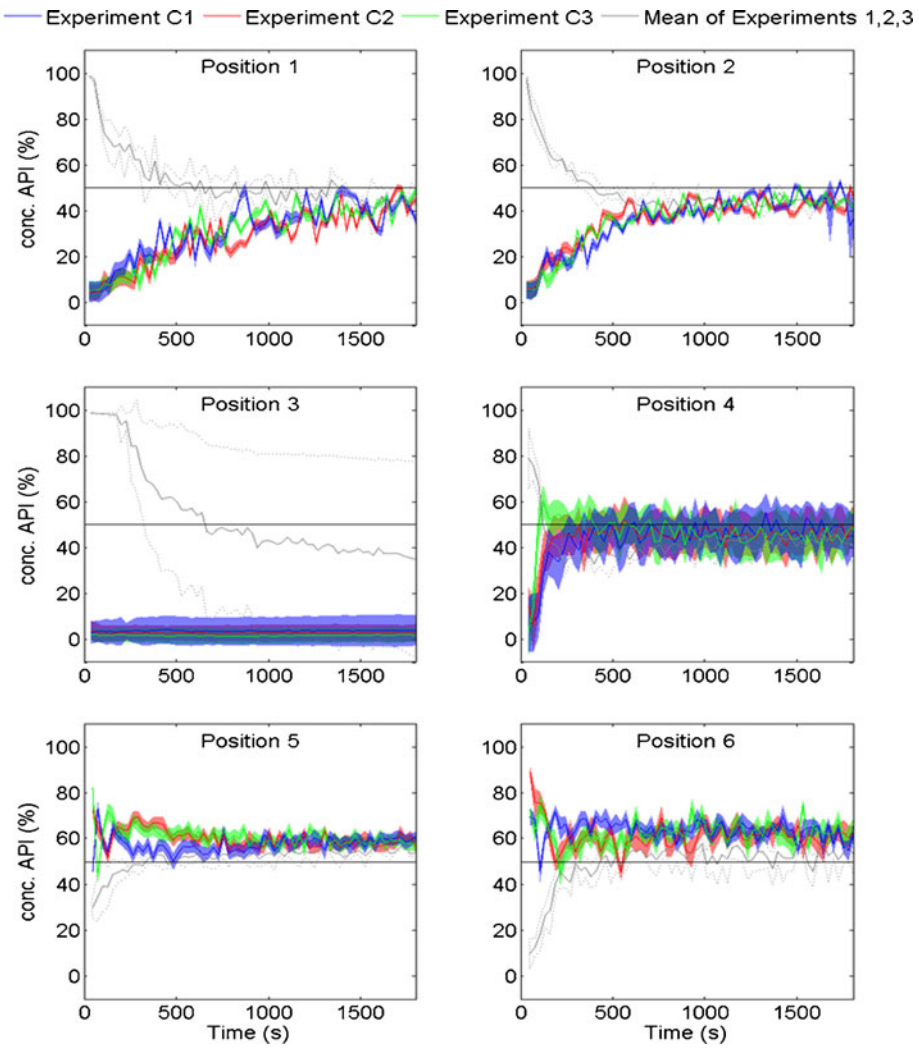

Fig. 7. Seventy grams ASA was loaded on top of 70 g LM. The experiments were repeated three times. The *solid lines* show the predicted values for the API, and the transparent area represents the respective 95% confidence interval of the prediction. The *black line* indicates the nominal value. The *dashed line* represents the mean of the experiments with reverse loading order (*i.e.*, Fig. 6). The *dotted lines* represent the standard deviation of the mean

Long-term dynamical studies should reveal if in both cases an identical final steady state could be reached.

The times until a steady state was reached estimated *via* MBSD as described in the "Determining Blending Dynamics, End Point, and Homogeneity" section are summarized in Table III. Choosing the loading order with ASA on top was favorable in terms of the required time. However, the reproducibility of the blending time was rather low.

Further, homogeneity of the blend cannot be predicted based on the time it takes to reach the stationary state, as in different locations different steady states may exist, *e.g.*, in the case of complete segregation. Therefore, the concentration levels must be monitored directly at various spatial locations. Numerous parameters of the blend homogeneity have been established with regard to thief probes (4), and various methods for determining the end point *via* NIR in combination

Table III. Times Until the Stationary State is Reached Estimated by MBSD Methodology

LM on ASA	Blending time (s)	ASA on LM	Blending time (s)
Experiment 1	441	Experiment C1	339
Experiment 2	472	Experiment C2	315
Experiment 3	414	Experiment C3	458
Mean	442±29	Mean	370±76

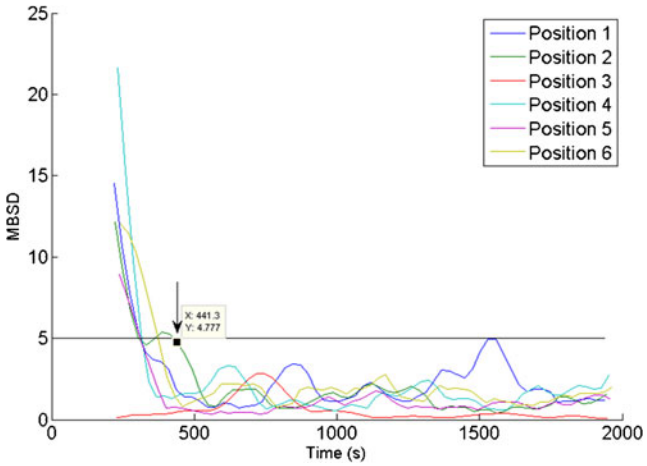

Fig. 8. MBSD used for the same experiment as in Figs. 3 and 5. The acceptance level of 5% is indicated by the *black line*. The *arrow* indicates the point in time, at which all positions are below the set level

with the nominal value are described in the literature (31). For a blend to be considered homogenous, two requirements must be met. First, the concentration should be within the same level everywhere, which can be tested by directly comparing the spectra. Secondly, the predicted concentrations should be within the specification of the nominal concentration, according to the fractions filled into the blender, for which a valid prediction model is needed (31).

However, NIR is limited by the sampling position and only provides information regarding the surface region of the blend. Our investigation offered the opportunity to examine the blend in different positions at the bottom and on the side. As such, concentration in the different positions, especially in the vertical direction, could be monitored. However, we still cannot "look" inside the blend.

The MBSD method for the first of the previously mentioned experiment is shown in Fig. 8. As can be seen, the positions exhibited different dynamics, and position 4 showed especially high blending dynamics. This was also true for the other experiments, which are not shown here. The time to reach steady state was defined when all positions (except position 3 due to its location at the corner of the blender) were below the set level of 5% at the same time. The resulting times (see Table III) provide estimates for the blending end point. As mentioned earlier, the estimated times until the stationary state was reached did not necessarily correspond with the overall homogeneity.

Different Fill Levels

The amount of powder used in the previously mentioned experiments was always 140 g, which corresponds to a fill level of H/D=0.35. To investigate the respective contribution of the convective and diffusive mixing mechanisms, the fill level was varied (H/D=0.25 (80 g), 0.35 (140 g), 0.50 (200 g), 0.60 (250 g), and 0.95 (400 g)). As for the vessel, diameter and height are the same and the H/D values are directly the fractions of volumes filled. Moreover, the fraction of ASA/LM was changed to 20:80, with LM on top. The loading order was not chosen in order to optimize the blending time, but to highlight the ASA transport within the powder bed.

Clearly, the blending time increased with the fill level, as shown in Fig. 9, which illustrates the mixing dynamics for position 2 at the bottom of the vessel. This position was chosen, since it clearly reveals the delay in reaching the nominal concentration. For every fill level, this position was covered by ASA at the start and should reach the nominal concentration of 20% ASA.

The estimated blending times according to the MBSD methodology are summarized in Table IV. A higher fill level resulted in a longer blending time. However, MBSD might not be suitable for this particular case since, at high fill levels, mixing and changes in the spectra are very slow. Therefore, if the same MBSD limit for all fill levels is used, the blending time for high levels may be underestimated.

Further, it was observed that, for a fill ratio of H/D=0.5, the blending time was unexpectedly long, when compared to other fill levels. An additional third run was performed, but showed the same result. The reason for this unexpected behavior is not clear and might be a result of a newly emerging powder flow pattern.

Of special interest is the experiment with H/D=0.95, with blending occurring rather fast in the beginning, *i.e.*, during the first 500 s. However, after that, a state was reached with nearly no change in the API concentration, but far from the nominal value. The concentrations are shown in Fig. 10 for the measurement position 2 at the bottom and positions 4, 5, 6, 7, and 9 on the side of the vessel (for a geometrical sketch, see Fig. 11).

The different time scales of convective and diffusive mixing could clearly be observed. First, ASA was at the bottom of the vessel (positions 2 and 4). During the first minutes of mixing, ASA was transported into the upper regions of the powder bed, as evidenced by the decrease in concentration in positions 2 and 4. Respectively, positions 5 and 6 showed a significant increase in concentration. However, the probes at positions 7 and 9 indicated no change in concentration. This can be interpreted as follows: ASA is first transported up in the powder bed due to the convective flow induced by the

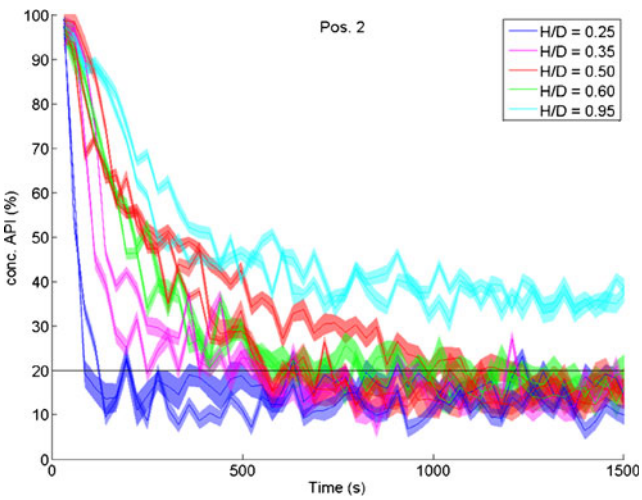

Fig. 9. Experiments with a different H/D ratio. The starting composition is always 80% LM on top of 20% ASA, as indicated by the *black line*. The *solid lines* are the PLS-predicted values, and the *transparent area* is the 95% confidence interval. Repetitions of the same experiments are shown in the same color. The experiment with H/D=0.5 was repeated three times because of its unexpected behavior

Table IV. Times Until a Stationary State is Reached Estimated by the MBSD Method

H/*D* ratio	Blending time (s)
0.25	297/302
0.35	338/368
0.50	344/544/645
0.60	475/480
0.95	436/505

The experiments are for a composition of 20% ASA below 80% LM for different fill levels. The different times arise from repetition experiments

impeller. Then, in the intermediate region of the vessel, ASA particles are transported upwards due to a segregation mechanism that was already observed above. However, for segregation to occur, the particle bed must be agitated, *i.e.*, a certain fluctuation level of particles (*i.e.*, diffusive motion) must occur. This is the case in a defined region above the stirrer, where an accumulation of ASA particles occurs (as seen in positions 5 and 6). However, in the top part of the vessel, the bed is stagnant and the granular temperature is very low. Thus, no accumulation of ASA occurs, as can be seen in Fig. 10. This effect is schematically shown in Fig. 11. After 73,000 s (approximately 20 h), the concentration still failed to reach a steady state. Furthermore, the NIR probes at positions 2 to 6 showed a concentration above the expected value of 20% ASA since a large portion of pure LM was still in the upper part of the vessel and showed no noticeable mixing at all.

The edge of the mixing zone is roughly at position 7. Above this position, very little mixing occurs. This can also be seen in Fig. 10. For a long time, only LM is seen

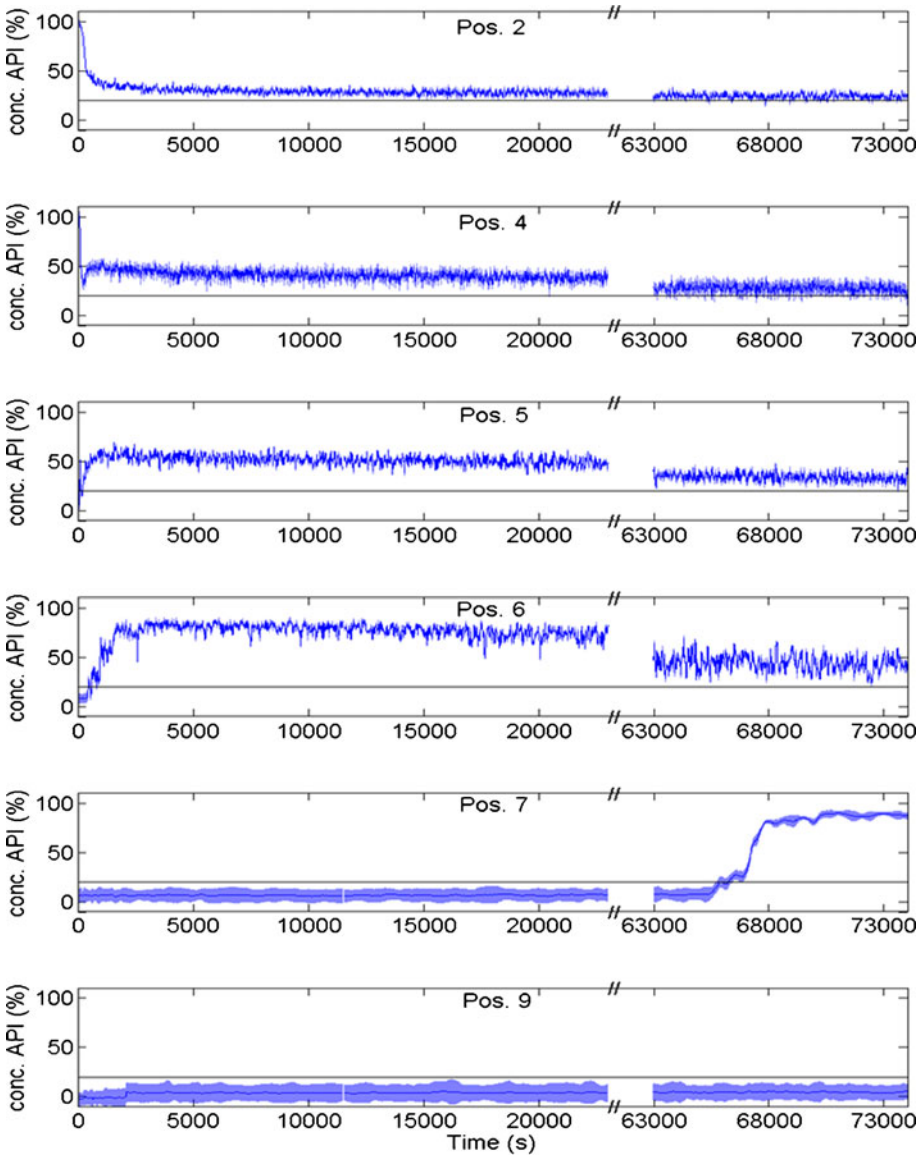

Fig. 10. Three hundred twenty grams LM were placed on top of 80 g ASA. The *black line* is the expected value of a perfect mixture. The *solid line* is the actual prediction by the PLS model. The *transparent area* represents the 95% confidence interval

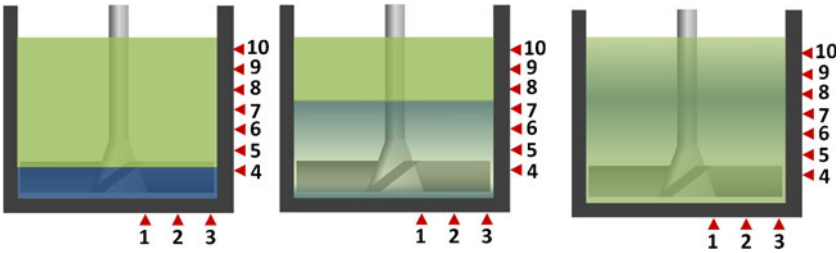

Fig. 11. Sketch of the mixing dynamics. The initial unmixed state is shown on the *left*. In the *center image*, ASA accumulates at positions *5–7*. After a long time, some ASA crystals are transported towards the top of the powder bed

by sensor 7. Concentration changes very slowly, indicating the slow movement of powder in front of the sensor at position 7. This is further backed by the large confidence interval, which indicates a low moving speed. However, at a certain time point, concentration rises continuously within 2,000 s to a different concentration level of about 90% ASA. As no rapid fluctuations can be seen, this might just be a volume containing mainly ASA crystals passing directly in front of the sensor. The overall powder movement is very slow and the receptive area of the probe is just slightly larger than the mean crystal diameter. Hence, we can just predict the concentration of LM and ASA in the small volume in front of the sensor, seeing the influence of stray crystals, if the movement of the powder bed is not sufficiently fast.

CONCLUSION

A multiprobe NIR setup in a laboratory-scale blender was used to monitor blending processes and to observe six different positions (quasi-)simultaneously. Developing a global model for all attached fibers and not separating the models makes the global model more robust and versatile. Moreover, by considering the confidence intervals of the predictions made *via* the PLS model, additional information regarding the investigated processes was obtained.

The multiple probe measurements allow a detailed analysis and understanding of powder mixing processes by gaining spatial information of the local powder concentration. For example, we demonstrated how loading order of the investigated materials resulted in different blending dynamics. Furthermore, increasing the fill level affected the mixing dynamics by creating different zones where different mixing effects dominate, *i.e.*, convective and diffusive mixing. Multiprobe NIR monitoring allows the detailed monitoring of these spatial mixing dynamics.

Multiple measurement positions open up yet another possibility for determining the blending end point. As opposed to comparing subsequently taken spectra, spectra at different positions can be used to calculate the standard deviation. Hence, it is possible to find the time point when a stationary state is reached.

Compared to traditional thief sampling, the advantage of the presented method is that there is no interference with the blending process itself of any kind. Nevertheless, as a drawback, samples can only be taken at the interface of the blend and vessel.

Additionally, it is important to place probes at locations where sufficient powder movement is obtained, as the sample volume of the NIR probe is small and a single stagnant crystal may bias the results. That is, a stagnant well-mixed area may be falsely reported as being demixed.

In summary, monitoring by multiple points showed that single-point measurements with NIR could lead to misinterpretations of the entire blending process. Hence, it is essential to choose a proper position—and even better multiple positions—when monitoring blending processes. Lastly, we would like to emphasize that, since NIR only provides information close to the positions of the probes, it is not possible to monitor effects that occur deeper inside the vessel.

REFERENCES

1. Mendez ASL, de Carli G, Garcia CV. Evaluation of powder mixing operation during batch production: application to operational qualification procedure in the pharmaceutical industry. Powder Technol. 2009;198:310–3.
2. Harnby N. An engineering view of pharmaceutical powder mixing. Pharm Sci Technol Today. 2000;3:303–9.
3. Remy B, Khinast JG, Glasser BJ. Discrete element simulation of free flowing grains in a four-bladed mixer. AIChE J. 2009;55:2035–48.
4. Stieß M. Mechanische Verfahrenstechnik—Partikeltechnologie 1. 3rd ed. Berlin: Springer; 2009.
5. Hogg R. Mixing and segregation in powder evaluation, mechanisms and processes. KONA Powder Part J. 2009;27:1–15.
6. Lekhal A, Girard KP, Brown MA, Kiang S, Glasser BJ, Khinast JG. Impact of agitated drying on crystal morphology: KCl–water system. Powder Technol. 2003;132:119–30.
7. Lekhal A, Girard KP, Brown MA, Kiang S, Khinast JG, Glasser BJ. The effect of agitated drying on the morphology of L-threonine (needle-like) crystals. Int J Pharm. 2004;270:263–77.
8. Poux M, Fayolle P, Betrand J, Bridoux D, Bousquet J. Powder mixing: some practical rules applied to agitated systems. Powder Technol. 1991;68:213–34.
9. Li H, McCarthy JJ. Controlling cohesive particle mixing and segregation. Phys Rev Lett. 2003;90:184301.
10. Acevedo D, Muliadi A, Giridhar A, Litster J, Romañach R. Evaluation of three approaches for real-time monitoring of roller compaction with near-infrared spectroscopy. AAPS PharmSciTech. 2012;13:1005–12.
11. Vanarase AU, Alcala M, Rozo JIJ, Muzzio FJ, Romanach RJ. Real-time monitoring of drug concentration in a continuous powder mixing process using NIR spectroscopy. Chem Eng Sci. 2010;65:5728–33.
12. Maltesen M, van de Weert M, Grohganz H. Design of experiments-based monitoring of critical quality attributes for the spray-drying process of insulin by NIR spectroscopy. AAPS PharmSciTech. 2012;13:747–55.
13. Duong NH, Arratia P, Muzzio F, Lange A, Timmermans J, Reynolds S. A homogeneity study using NIR spectroscopy: tracking magnesium stearate in Bohle bin-blender. Drug Dev Ind Pharm. 2003;29:679–87.

14. Reich G. Near-infrared spectroscopy and imaging: basic principles and pharmaceutical applications. Adv Drug Deliv Rev. 2005;57:1109–43.
15. Roggo Y, Chalus P, Maurer L, Lema-Martinez C, Edmond A, Jent N. A review of near infrared spectroscopy and chemometrics in pharmaceutical technologies. J Pharm Biomed Anal. 2007;44:683–700.
16. Sekulic SS, Ward II HW, Brannegan DR, Stanley ED, Evans CL, Sciavolino ST, Haily PA, Aldridge PK. On-line monitoring of powder blend homogeneity. Anal Chem. 1996;68:509–13.
17. Blanco M, Baó RG, Bertran E. Monitoring powder blending in pharmaceutical processes by use of near infrared spectroscopy. Talanta. 2002;56:203–12.
18. Berntsson O, Danielsson L-G, Lagerholm B, Folestad S. Quantitative in-line monitoring of powder blending by near infrared reflection spectroscopy. Powder Technol. 2002;123:185–93.
19. El-Hagrasy AS, Drennen III JK. A process analytical technology approach to near-infrared process control of pharmaceutical powder blending. Part III: quantitative near-infrared calibration for prediction of blend homogeneity and characterization of powder mixing kinetics. J Pharm Sci. 2005;95:422–34.
20. Abrahamsson C. Time-Resolved Spectroscopy for Pharmaceutical Applications. Ph.D. thesis, Atomic Physics Division, Department of Physics, Lund Institute of Technology; 2005.
21. Karande AD, Liew CV, Heng PWS. Calibration sampling paradox in near infrared spectroscopy: a case study of multicomponent powder blend. Int J Pharm. 2010;395:91–7.
22. Remy B, Glasser BJ, Khinast JG. The effect of mixer properties and fill level on granular flow in a bladed mixer. AIChE J. 2010;56:336–53.
23. Radl S, Kalvoda E, Glasser BJ, Khinast JG. Mixing characteristics of wet granular matter in a bladed mixer. Powder Technol. 2010;200:171–89.
24. Brone D, Alexander A, Muzzio FJ. Quantitative characterization of mixing dry powders in V-blenders. AIChE J. 1998;44:271–8.
25. Koller DM, Posch A, Hörl G, Voura C, Radl S, Urbanetz N, Fraser SD, Tritthart W, Reiter F, Schlingmann M, Khinast JG. Continuous quantitative monitoring of powder mixing dynamics by near-infrared spectroscopy. Powder Technol. 2011;205:87–96.
26. El-Hagrasy AS, Morris HR, D'Amico F, Lodder RA, Drennen III JK. Near-infrared spectroscopy and imaging for the monitoring of powder blend homogeneity. J Pharm Sci. 2001;90:1298–307.
27. Witt W, Köhler U, List J. Experiences with dry dispersion and high-speed image analysis for size and shape characterisation. Particulate System Analysis, Stratford-upon-Avon; 2005. p. 1–5.
28. Kessler W. Multivariate Datenanalyse für die Pharma-, Bio- und Prozessanalytik. Weinheim: Wiley-VCH; 2007.
29. Wold S, Sjöström M, Eriksson L. PLS-regression: a basic tool of chemometrics. Chemometr Intell Lab Syst. 2001;58:109–30.
30. Momose W, Imai K, Yokota S, Yonemochi E, Terada K. Process analytical technology applied for end-point detection of pharmaceutical blending by combining two calibration free methods: simultaneously monitoring specific near-infrared peak intensity and moving block standard deviation. Powder Technol. 2011;210:122–31.
31. Shi Z, Cogdill RP, Short SM, Anderson CA. Process characterization of powder blending by near-infrared spectroscopy: blend endpoints and beyond. J Pharm Biomed Anal. 2008;47:738–45.